mater.scichina.com link.springer.com

Published online 28 February 2023 | https://doi.org/10.1007/s40843-022-2371-9
Sci China Mater 2023, 66(6): 2192–2198

Recycling of garnet solid electrolytes with lithium-dendrite penetration by thermal healing

Shaojie Chen[1†], Xiangchen Hu[1†], Lu Nie[1], Yi Yu[1,3] and Wei Liu[1,2,3*]

ABSTRACT Solid-state lithium metal batteries (SSLMBs) have attracted a lot of interest owing to their high safety and high energy density potential. However, the growth of lithium dendrite in solid electrolytes still hinders practical applications of SSLMBs. In this study, we develop a simple heat treatment method for reviving and recycling garnet oxide electrolytes with Li dendrite penetration. Interestingly, the recovered garnet electrolyte exhibits higher relative density, enhanced ionic conductivity and improved critical current density compared with the pristine one. The thermal healing is due to the products of the reaction between dendritic Li metal and air that contribute to the further densification of garnet electrolytes during heat treatment. This work demonstrates a new way to recycle garnet electrolytes, which may further extend to other various solid electrolytes.

Keywords: garnet electrolyte, lithium dendrite, lithium metal battery, dendrite healing

INTRODUCTION

Metallic lithium (Li) is considered the ultimate anode material of next-generation high-performance energy storage systems due to its ultrahigh theoretical specific capacity (3860 mA h g^{-1}), ultralow electrochemical potential (−3.04 V *vs.* the standard hydrogen electrode), and low density (0.534 g cm^{-3}) [1–6]. Solid-state lithium metal batteries (SSLMBs) with Li metal as the high-capacity anode are becoming one of the most promising candidates for next-generation energy storage devices due to their high safety and potentially high energy density. SSLMBs are expected to be the future of conventional lithium-ion batteries (LIBs) [7,8]. It is predicted that the global demand for solid-state batteries will reach 500 GW h by 2030. Therefore, recycling of SSLMBs is of great significance. However, currently adopted approaches for battery recycling mainly focus on LIBs, while only a few studies have explored SSLMB recycling [9–17].

Meanwhile, there is still limited development of SSLMBs due to the severe safety issues caused by uncontrolled Li dendrite formation and growth [18,19]. Garnet oxide electrolyte $Li_7La_3Zr_2O_{12}$ (LLZO) has been considered one of the most promising solid electrolytes for high-safety and high-performance solid-state batteries [20–24]. According to Monroe and Newman's prediction [25,26], garnet oxide electrolyte is able to prevent the growth of Li dendrites due to its high shear modulus (~60 GPa) and Young's modulus (~150 GPa). However, several recent studies have found that at high current densities, Li dendrites still penetrate through LLZO electrolytes [27–29]. There are several possible mechanisms of dendrite formation and growth inside ceramic solid electrolytes (CSEs). It is widely believed that Li dendrites first nucleate at the Li/CSE interface due to the uneven Li flux distribution caused by poor contact. The dendrites will then preferentially propagate along the voids and grain boundaries in polycrystalline CSEs because of their low mechanical strengths [30]. Moreover, the electronic conductivity of CSEs is also likely to facilitate the formation of Li dendrites directly inside the CSEs [31,32]. Currently, a vast majority of studies concentrate on investigating the dendrite formation mechanism and interface modification of Li/CSE [33–45]. However, at high current densities or after long cycling, Li dendrites or Li deposits still form in CSEs, while strategies focusing on healing or recycling CSEs with Li dendrite penetration are rarely reported [46–48]. Recently, Wang *et al.* [49] reported a recovery strategy to recycle shorted LLZO pellets *via* one-step annealing.

In this work, we demonstrate a facile method for healing and recycling garnet electrolytes with Li dendrites through heat treatment. Excitingly, the recycled garnet ceramic pellets have increased ionic conductivity with higher relative density. The higher conductivity is attributed to the dendrite-derived species in the grain boundaries that are able to promote further densification of garnet electrolyte pellets during the thermal healing process as sintering aids (Fig. 1a). Compared with pristine garnet electrolyte pellets, the relative density of the recycled garnet pellets is improved from 90.9% to 95.3%, while its ionic conductivity is improved from 0.39 to 0.62 mS cm^{-1}. A higher critical current density (CCD) is achieved as a result of the enhanced relative density and ionic conductivity, suggesting a better suppression effect on Li dendrite penetration.

EXPERIMENTAL SECTION

LLZTO pellet synthesis

$Li_{6.4}La_3Zr_{1.4}Ta_{0.6}O_{12}$ (LLZTO) powders were prepared by a traditional solid-state reaction. First, $LiOH{\cdot}H_2O$ (≥98%, Aladdin), Ta_2O_5 (99.99%, Macklin), ZrO_2 (99.99%, Aladdin), and La_2O_3 powders (99.99%, Macklin) were ball milled in isopropanol at

[1] School of Physical Science and Technology, ShanghaiTech University, Shanghai 201210, China
[2] Key Laboratory of Advanced Energy Materials Chemistry (Ministry of Education), Nankai University, Tianjin 300071, China
[3] Shanghai Key Laboratory of High-resolution Electron Microscopy, ShanghaiTech University, Shanghai 201210, China
† These authors contributed equally to this work.
* Corresponding author (email: liuwei1@shanghaitech.edu.cn)

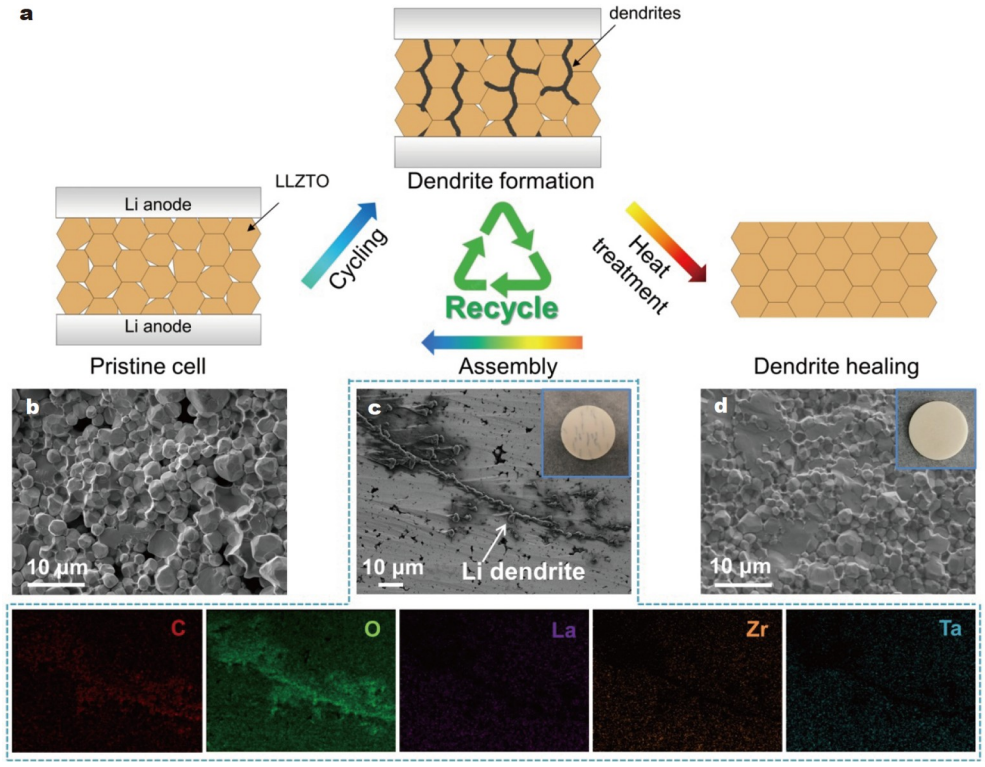

Figure 1 Utilization and recycling process for LLZTO solid electrolytes. (a) Schematic diagram showing the formation and healing process for Li dendrites. (b) Cross-sectional SEM image of the pristine LLZTO pellet. (c) Cross-sectional SEM image and the corresponding EDS mapping of the LLZTO pellet with dendrites (inset: optical picture of the LLZTO pellet with dendrites). (d) Cross-sectional SEM image of the recycled LLZTO pellet (inset: optical picture of the recycled LLZTO pellet).

600 r min^{-1} for 6 h according to the above stoichiometric ratio. Then 20 wt% excess of LiOH·H_2O was used to compensate for the lithium loss that occurs during the high-temperature calcination process. The mixture was then dried and calcinated in air at 950°C for 6 h to synthesize LLZTO powders. To obtain garnet ceramic pellets, 2 wt% γ-Al_2O_3 powders (99.99%, Energy Chemical) were added to the LLZTO powders, and the mixture was uniaxially pressed into green pellets. The green pellets were then sintered in air at 1100°C for 12 h while covered with LLZTO mother powders. Finally, the LLZTO pellet used in this experiment was carefully polished with sand papers to remove the surface impurities. The density of the LLZTO pellet was measured by Archimedes' method. A theoretical density of 5.5 g cm^{-3} was used to calculate the relative density of the different samples.

Li dendrite healing through heat treatment

The short-circuited Li symmetric cell was disassembled in air, and then the Li anodes were polished away using sand papers. The LLZTO pellets with Li dendrites were stored in air (humidity: ~50%) for 48 h and then heated at 1000°C for 12 h for dendrite healing.

Characterizations

High-resolution X-ray diffraction (HRXRD) was carried out using an X-ray diffractometer PANalytical EMPYREAN with a Cu Kα (λ = 1.5418 Å). Scanning electron microscopy (SEM) images were recorded using a JEOL JSM-7800F. For better distinction of the Li dendrites in the LLZTO pellet, the LLZTO pellet cross-section was polished using an ion beam (JEOL, IB-19520CCP). Transmission electron microscopy (TEM) was conducted using a JEOL F200 equipped with a field emission gun. The cross-sectional TEM specimens were prepared by using focused ion beam (FIB) equipment (JEOL JIB-4700F).

Electrochemical measurements

The blocking electrode was formed *via* sputtering gold for 5 min on each side of the LLZTO pellet to measure the ionic conductivity. The electrochemical impedance spectrum (EIS) measurement was performed through a Biologic VMP300 potentiostat over a frequency range from 1 to 7 MHz. To assemble Li symmetric cells, Li foil (Adamas-beta®) was first melted on a hotplate at ~250°C. LLZTO pellets were then rubbed in molten Li until the pellets were completely wetted, followed by cooling down and coin-cell assembling. The CCD value was measured using the LAND system and Neware battery cycler, starting with an initial current density of 0.02 mA cm^{-2} and increasing in steps of 0.02 mA cm^{-2}. The charge and discharge times were set to be 30 min.

RESULTS AND DISCUSSION

Ta-doped LLZO (LLZTO) was chosen in this experiment owing to its high ionic conductivity and high chemical stability toward the Li anode. Fig. 1b displays the cross-sectional SEM image of the pristine LLZTO ceramic pellet, which shows a microstructure with plenty of intergranular fractures. Following a short-circuit, Li dendrites could be found inside the LLZTO pellets (Fig. 1c). The corresponding energy dispersive spectroscopy (EDS) mapping shows that the dendrite region was rich in C and O elements and lacking in La, Zr and Ta elements due to

the reaction between Li dendrite and air during the disassembling process in air [30]. Additionally, several black lines appeared on the surface, as shown from the optical picture of the LLZTO pellet with dendrites. After heat treatment, the black lines disappeared (inset of Fig. 1d), indicating the healing of Li dendrites. The cross-sectional SEM image of the recycled LLZTO pellet presents a denser microstructure with massive transgranular fractures (Fig. 1d).

The reaction products between Li dendrite and air may influence the recycling process. The reaction products were characterized by low-angle grazing incidence HRXRD. As shown in Fig. 2a, the pristine LLZTO pellet exhibited a standard cubic garnet crystal structure, while for the LLZTO pellet with dendrite, some peaks corresponding to LiOH and Li_2CO_3 appeared after contacting with air. Similar reports from literature show that LiOH and Li_2CO_3 are the reaction products between Li dendrites and air [30]. Additionally, the Li_2CO_3 and LiOH peaks all disappeared in the recycled LLZTO pellet, implying successful dendrite removal. The dendrite-derived LiOH and Li_2CO_3 species formed through the reactions between Li dendrites and air as follows:

$2Li + 2H_2O = 2LiOH + H_2$,

$2LiOH + CO_2 = Li_2CO_3 + H_2O$.

To further investigate the product of the reaction between the dendrites and air, FIB-TEM was employed. Li dendrites at grain boundaries have darker contrast in SEM; hence it is possible to prepare a cross-sectional specimen of the Li dendrite region. To make sure the selected area contains Li dendrites, the LLZTO pellets were further confirmed by using an optical microscope before thinning the lamella. The black areas shown in Fig. 2b represent the regions with dendrites, one of which was selected for TEM sample preparation. Fig. 2c shows the TEM image of the specimen obtained from the red circle area in Fig. 2b. There are numerous voids and grain boundaries between LLZTO

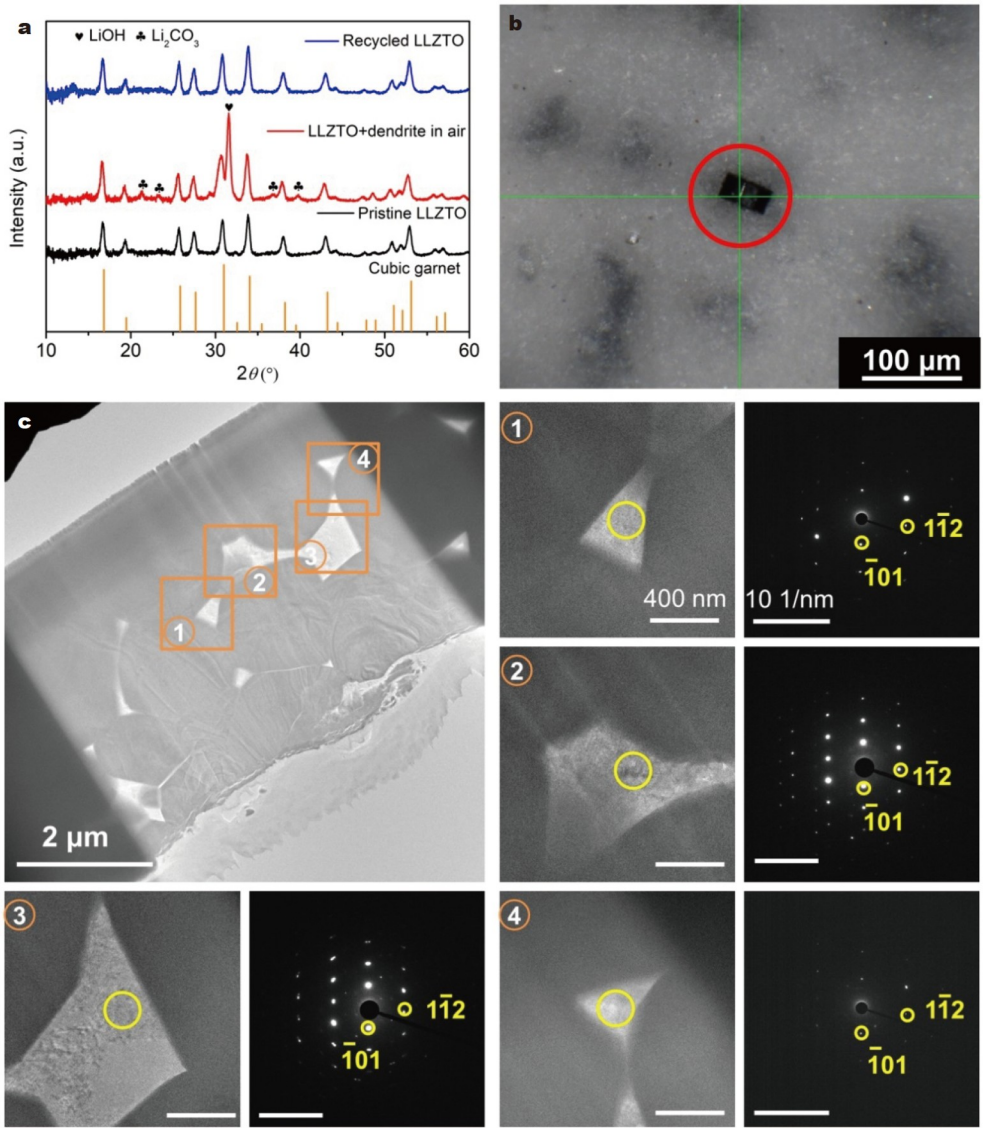

Figure 2 Characterizations of the dendrite derivatives. (a) HRXRD patterns of various LLZTO samples. (b) Optical image of the surface of the LLZTO pellet with dendrites. The FIB specimen was picked up from the red circle region. (c) TEM images of the LLZTO pellet with dendrites. The four regions highlighted with orange squares were observed to portray the reaction product between Li dendrites and air. The SAED patterns were taken from the area within orange circles in regions 1–4, respectively.

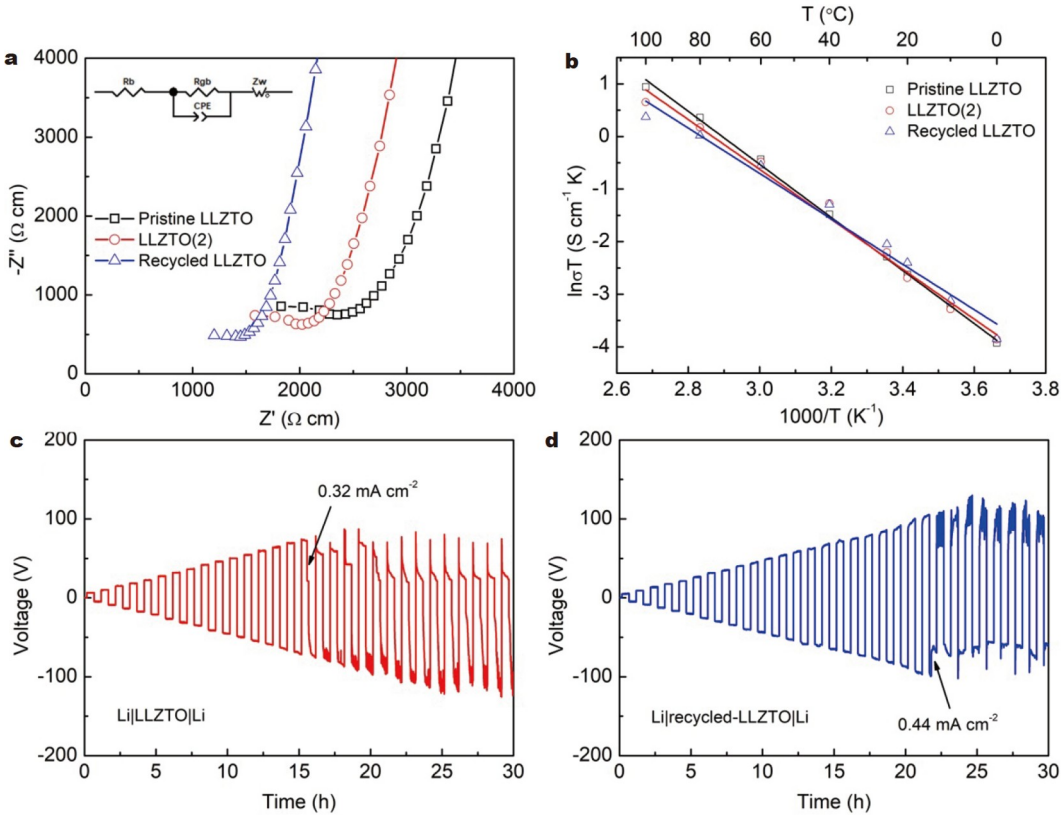

Figure 3 Electrochemical performances of different LLZTO samples. (a) EIS curves of different LLZTO pellets. (b) Arrhenius plots of different LLZTO pellets. (c) Li plating-stripping performances of Li|LLZTO|Li symmetric cell at different current densities. (d) Li plating-stripping performances of Li|recycled-LLZTO|Li symmetric cell at different current densities.

grains, which are the breeding grounds for dendrite growth. Therefore, four different void regions were investigated. The corresponding selected area electron diffraction (SAED) patterns are all consistent with LiOH viewed along the zone axis [131], indicating that in this region, the product of the reaction between Li dendrites and the air is LiOH, which is in agreement with the HRXRD result.

Li dendrites tend to grow along the grain boundaries of the LLZTO pellets; hence exposure to air leads to the *in-situ* formation of dendrite-derived LiOH and Li_2CO_3 inside the grain boundaries and voids. We suspect that the LiOH and Li_2CO_3 may contribute to the healing and recycling of the shorted LLZTO pellets as sintering additives, leading to better electrochemical performances. As shown in Fig. S1, abnormal grain growth of LLZTO pellets occurred when the recycling temperature was 1100°C. Therefore, we chose a lower temperature (1000°C) for the recycling process. The ionic conductivities of LLZTO pellets were measured by using two ion-blocking electrodes. Considering that heat treatment may also influence ionic conductivity, LLZTO pellets without dendrite penetration were also subjected to the same heat treatment process and were named "LLZTO(2)". The EIS curves of the pristine LLZTO, LLZTO(2) and recycled LLZTO are shown in Fig. 3a. The curves are characterized by a semicircle at high frequencies and an oblique line at low frequencies. Since the semicircle does not start from the origin, the real axis intercepts of the semicircle at higher and lower frequencies represent the LLZTO bulk resistance and grain boundary resistance, respectively. As displayed in Table 1, the ionic conductivities for pristine LLZTO, LLZTO (2) and recycled LLZTO were 0.39, 0.45 and 0.62 mS cm^{-1}, respectively. One can see that heat treatment enhanced the ionic conductivity of LLZTO pellets without dendrites to a certain extent. Importantly, the recycled LLZTO exhibited the highest ionic conductivity, indicating that the existence of LiOH and Li_2CO_3 could lead to better densification and, thus, a higher ionic conductivity, which was in agreement with the relative density results. The relative densities of the pristine LLZTO, LLZTO(2) and recycled LLZTO were 90.9%, 92.9% and 95.3%, respectively. Moreover, as presented in Fig. 3b, the activation energies for the pristine LLZTO, LLZTO(2) and recycled LLZTO were 0.43 ± 0.01, 0.41 ± 0.02 and 0.37 ± 0.02 eV, respectively. The recycled LLZTO pellets also exhibited the lowest ion-diffusion barrier. The CCD, at which the cell would abruptly short-circuit, is a vital parameter for the LLZTO electrolyte. As shown in Fig. 3c, d, the CCD values for the pristine LLZTO and recycled LLZTO were 0.32 and 0.44 mA cm^{-2}, respectively, showing that the recycled LLZTO had better inhibition of dendrite growth.

The sintering roles of LiOH and Li_2CO_3 were further inves-

Table 1 Performances of various LLZTO solid electrolytes

Samples	Relative density	σ (mS cm^{-1})	Active energy (eV)
Pristine LLZTO	90.9%	0.39	0.43 ± 0.01
LLZTO(2)	92.9%	0.45	0.41 ± 0.02
Recycled LLZTO	95.3%	0.62	0.37 ± 0.02

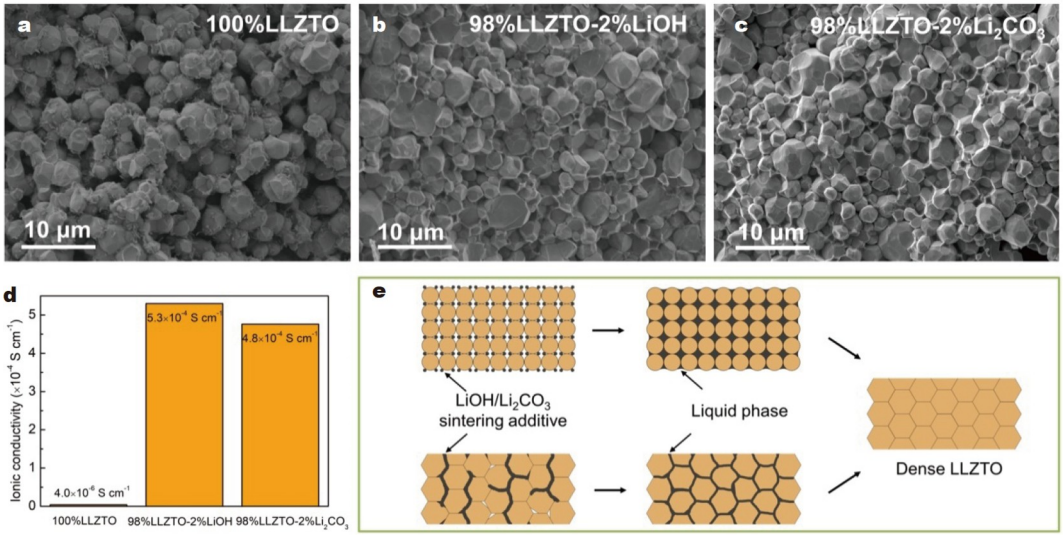

Figure 4 Effects of LiOH and Li_2CO_3 sintering aids. (a–c) Cross-sectional SEM images of the 100%LLZTO, 98%LLZTO-2%LiOH and 98%LLZTO-2%Li_2CO_3 pellets. (d) Corresponding ionic conductivities. (e) Assisted sintering mechanism of Li dendrite derivatives.

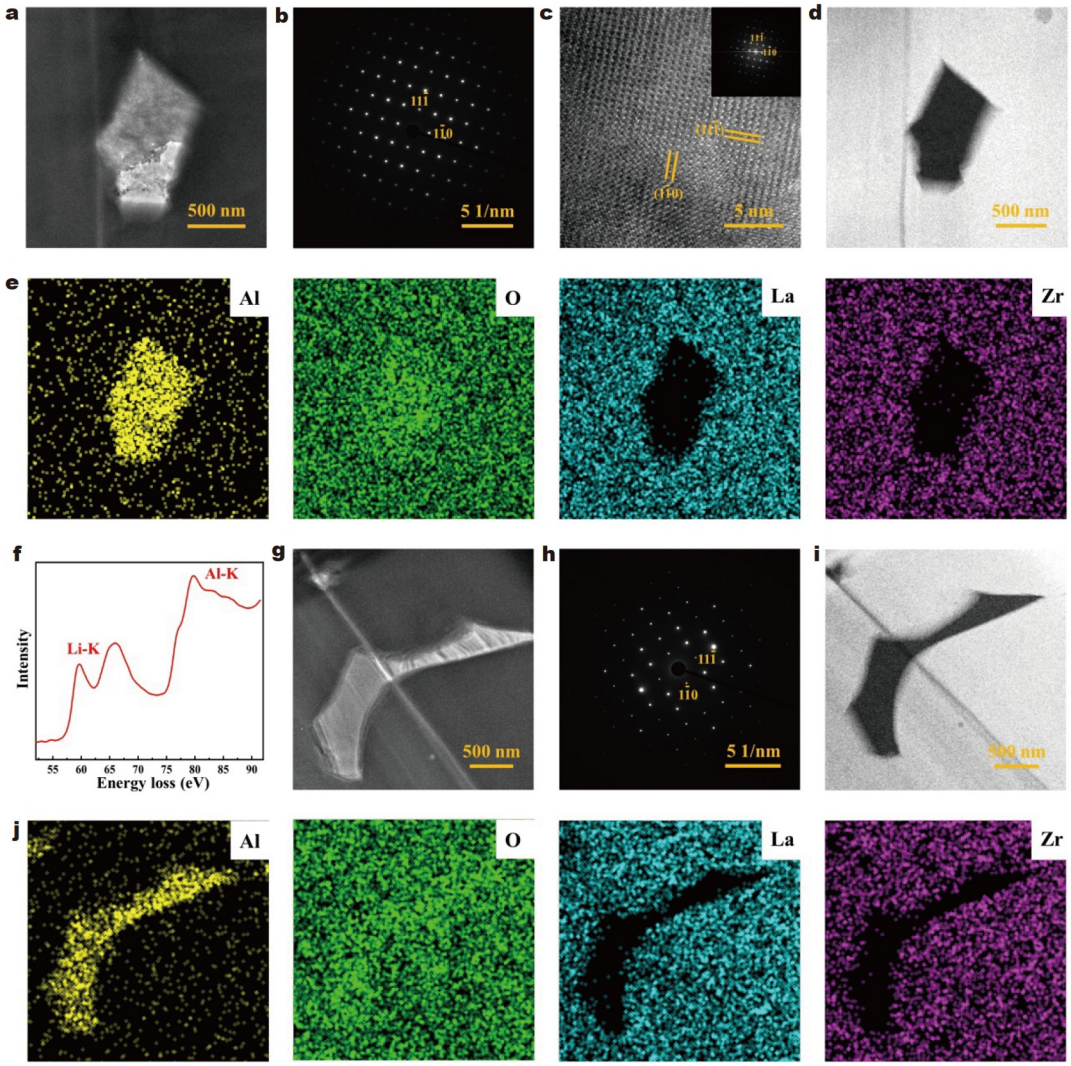

Figure 5 TEM characterization of the second phase of (a–f) 98%LLZTO-2%LiOH and (g–j) 98%LLZTO-2%Li_2CO_3, respectively. (a, g) Morphologies of α-Li_5AlO_4 (grain boundary) and LLZTO (grain). (b, h) SAED patterns of α-Li_5AlO_4 along the [112] zone axis. (c) HRTEM image of α-Li_5AlO_4. (d, i) ADF-scanning TEM images of α-Li_5AlO_4. (e, j) Corresponding EDS mapping. (f) EELS result for the grain boundary in (a).

tigated. LLZTO pellets without sintering additives and with 2 wt% LiOH or 2 wt% Li_2CO_3 powders were prepared, named "100%LLZTO", "98%LLZTO-2%LiOH", and "98%LLZTO-2% Li_2CO_3", respectively. The 100%LLZTO sample displayed a loose cross-sectional morphology (Fig. 4a), while both 98%LLZTO-2% LiOH and 98%LLZTO-2%Li_2CO_3 displayed a dense microstructure (Fig. 4b, c), which proved the previous conjecture that LiOH and Li_2CO_3 could work as sintering additives. As displayed in Fig. S2 and Fig. 4d, the ionic conductivities for the 100%LLZTO, 98%LLZTO-2%LiOH and 98%LLZTO-2%Li_2CO_3 were 4.0×10^{-6}, 5.3×10^{-4} and 4.7×10^{-4} S cm^{-1}, demonstrating that adding LiOH and Li_2CO_3 to LLZTO could effectively improve its relative density and ionic conductivity.

Li dendrites tend to penetrate through the grain boundaries and voids in LLZTO ceramic electrolytes because of their low mechanical strengths. The *in-situ* formed Li dendrite derivatives can promote sintering during heat treatment, thus strengthening the weak regions and increasing the relative density. The assisted sintering mechanism of Li dendrite derivatives (LiOH and Li_2CO_3) is displayed in Fig. 4e. In the high-temperature sintering process, LiOH and Li_2CO_3 first decompose into Li_2O. As a sintering aid, Li_2O also proved to be a good binder, which could lead to liquid phase sintering behavior [50]. The liquid phases formed in grain boundaries could eliminate the residual pores and improve the relative density.

To investigate the microstructure of the second phase for the 98%LLZTO-2%LiOH and 98%LLZTO-2%Li_2CO_3 samples, TEM characterization was carried out. Fig. 5a shows the morphology of the LLZTO grains and grain boundaries of the 98%LLZTO-2%LiOH sample. Due to the difference in atomic number, LLZTO grains have darker contrast. Fig. 5b displays the SAED pattern of the grain boundary region, which matches α-Li_5AlO_4 along the zone axis [112], while Fig. 5c shows the corresponding HRTEM image of the grain boundaries. The annular dark-field (ADF) image (Fig. 5d) and the corresponding EDS mapping (Fig. 5e) show the elemental distribution of the grain boundaries. Unlike the LLZTO grains, Al and O elements are mainly distributed in this region. To further confirm the chemical composition of the second phase, electron energy-loss spectroscopy (EELS) was conducted and shown in Fig. 5f. Li-K and Al-K edges can be observed in the spectrum. The TEM characterization of the 98%LLZTO-2%Li_2CO_3 sample has similar results. The SAED pattern (Fig. 5h) and EDS mapping (Fig. 5j) demonstrate that the crystal structure of this region is also α-Li_5AlO_4. The α-Li_5AlO_4 second phase can fill the original voids and thus enhance relative density, which also proves that the liquid sintering process exists.

CONCLUSIONS

In summary, we applied a simple method based on heat treatment for healing dendrites and recycling LLZTO electrolytes. The recycled LLZTO pellets exhibited a denser microstructure, enhanced ionic conductivity, and higher CCD value. Through HRXRD and FIB-TEM characterizations, the reaction product between Li dendrites and air was identified to be LiOH and Li_2CO_3, which could contribute to further densification of the LLZTO electrolyte during heat treatment. This work provides a new recycling method for CSEs.

Received 15 November 2022; accepted 20 December 2022; published online 28 February 2023

1 Lin D, Liu Y, Cui Y. Reviving the lithium metal anode for high-energy batteries. Nat Nanotech, 2017, 12: 194–206
2 Guo Y, Li H, Zhai T. Reviving lithium-metal anodes for next-generation high-energy batteries. Adv Mater, 2017, 29: 1700007
3 Ji X, Zhang Y, Cao M, *et al.* Advanced inorganic/polymer hybrid electrolytes for all-solid-state lithium batteries. J Adv Ceram, 2022, 11: 835–861
4 Liu H, Cheng X, Zhang R, *et al.* Mesoporous graphene hosts for dendrite-free lithium metal anode in working rechargeable batteries. Trans Tianjin Univ, 2020, 26: 127–134
5 Hu Q, Sun Z, Nie L, *et al.* High-safety composite solid electrolyte based on inorganic matrix for solid-state lithium-metal batteries. Mater Today Energy, 2022, 27: 101052
6 Zheng J, Zhang W, Huang C, *et al. In-situ* polymerization with dual-function electrolyte additive toward future lithium metal batteries. Mater Today Energy, 2022, 26: 100984
7 Zhao N, Khokhar W, Bi Z, *et al.* Solid garnet batteries. Joule, 2019, 3: 1190–1199
8 Chen S, Zhang J, Nie L, *et al.* All-solid-state batteries with a limited lithium metal anode at room temperature using a garnet-based electrolyte. Adv Mater, 2021, 33: 2002325
9 Jia K, Wang J, Ma J, *et al.* Suppressed lattice oxygen release *via* Ni/Mn doping from spent $LiNi_{0.5}Mn_{0.3}Co_{0.2}O_2$ toward high-energy layered-oxide cathodes. Nano Lett, 2022, 22: 8372–8380
10 Jiao M, Zhang Q, Ye C, *et al.* Isolating contiguous Fe atoms by forming a Co–Fe intermetallic catalyst from spent lithium-ion batteries to regulate activity for zinc-air batteries. ACS Nano, 2022, 16: 13223–13231
11 Jiao M, Zhang Q, Ye C, *et al.* Recycling spent $LiNi_{1-x-y}Mn_xCo_yO_2$ cathodes to bifunctional NiMnCo catalysts for zinc-air batteries. Proc Natl Acad Sci USA, 2022, 119: e2202202119
12 Ma J, Wang J, Jia K, *et al.* Adaptable eutectic salt for the direct recycling of highly degraded layer cathodes. J Am Chem Soc, 2022, 144: 20306–20314
13 Wang J, Ma J, Jia K, *et al.* Efficient extraction of lithium from anode for direct regeneration of cathode materials of spent Li-ion batteries. ACS Energy Lett, 2022, 7: 2816–2824
14 Wang J, Zhang Q, Sheng J, *et al.* Direct and green repairing of degraded $LiCoO_2$ for reuse in lithium-ion batteries. Natl Sci Rev, 2022, 9: nwac097
15 Azhari L, Bong S, Ma X, *et al.* Recycling for all solid-state lithium-ion batteries. Matter, 2020, 3: 1845–1861
16 Schwich L, Küpers M, Finsterbusch M, *et al.* Recycling strategies for ceramic all-solid-state batteries—Part I: Study on possible treatments in contrast to Li-ion battery recycling. Metals, 2020, 10: 1523
17 Tan DHS, Chen Z. Sustainable design of fully recyclable all solid-state batteries. MRS Bull, 2020, 45: 990–991
18 Yuan K, Tu T, Shen C, *et al.* Self-ball milling strategy to construct high-entropy oxide coated $LiNi_{0.8}Co_{0.1}Mn_{0.1}O_2$ with enhanced electrochemical performance. J Adv Ceram, 2022, 11: 882–892
19 Sun M, Zeng Z, Peng L, *et al.* Ultrathin polymer electrolyte film prepared by *in situ* polymerization for lithium metal batteries. Mater Today Energy, 2021, 21: 100785
20 Gonzalez Puente PM, Song S, Cao S, *et al.* Garnet-type solid electrolyte: Advances of ionic transport performance and its application in all-solid-state batteries. J Adv Ceram, 2021, 10: 933–972
21 Zheng C, Su J, Song Z, *et al.* Improvement of density and electrochemical performance of garnet-type $Li_7La_3Zr_2O_{12}$ for solid-state lithium metal batteries enabled by W and Ta co-doping strategy. Mater Today Energy, 2022, 27: 101034
22 Chen S, Nie L, Hu X, *et al.* Ultrafast sintering for ceramic-based all-solid-state lithium-metal batteries. Adv Mater, 2022, 34: 2200430
23 Chen S, Hu X, Bao W, *et al.* Low-sintering-temperature garnet oxides by conformal sintering-aid coating. Cell Rep Phys Sci, 2021, 2: 100569
24 Wu W, Song Z, Dai Y, *et al.* Magnetic actuation enables programmable lithium metal engineering. Adv Energy Mater, 2022, 12: 2200999
25 Monroe C, Newman J. The impact of elastic deformation on deposition kinetics at lithium/polymer interfaces. J Electrochem Soc, 2005, 152: A396
26 Chen R, Li Q, Yu X, *et al.* Approaching practically accessible solid-state

batteries: Stability issues related to solid electrolytes and interfaces. Chem Rev, 2020, 120: 6820–6877
27 Krauskopf T, Dippel R, Hartmann H, *et al.* Lithium-metal growth kinetics on LLZO garnet-type solid electrolytes. Joule, 2019, 3: 2030–2049
28 Mo F, Ruan J, Sun S, *et al.* Inside or outside: Origin of lithium dendrite formation of all solid-state electrolytes. Adv Energy Mater, 2019, 9: 1902123
29 Chen S, Nie Z, Tian F, *et al.* The influence of surface chemistry on critical current density for garnet electrolyte. Adv Funct Mater, 2022, 32: 2113318
30 Cheng EJ, Sharafi A, Sakamoto J. Intergranular Li metal propagation through polycrystalline $Li_{6.25}Al_{0.25}La_3Zr_2O_{12}$ ceramic electrolyte. Electrochim Acta, 2017, 223: 85–91
31 Han F, Westover AS, Yue J, *et al.* High electronic conductivity as the origin of lithium dendrite formation within solid electrolytes. Nat Energy, 2019, 4: 187–196
32 Song Y, Yang L, Zhao W, *et al.* Revealing the short-circuiting mechanism of garnet-based solid-state electrolyte. Adv Energy Mater, 2019, 9: 1900671
33 Kazyak E, Garcia-Mendez R, LePage WS, *et al.* Li penetration in ceramic solid electrolytes: *Operando* microscopy analysis of morphology, propagation, and reversibility. Matter, 2020, 2: 1025–1048
34 Porz L, Swamy T, Sheldon BW, *et al.* Mechanism of lithium metal penetration through inorganic solid electrolytes. Adv Energy Mater, 2017, 7: 1701003
35 Liu X, Garcia-Mendez R, Lupini AR, *et al.* Local electronic structure variation resulting in Li 'filament' formation within solid electrolytes. Nat Mater, 2021, 20: 1485–1490
36 Fu KK, Gong Y, Liu B, *et al.* Toward garnet electrolyte-based Li metal batteries: An ultrathin, highly effective, artificial solid-state electrolyte/metallic Li interface. Sci Adv, 2017, 3: e1601659
37 Liang JY, Zeng XX, Zhang XD, *et al.* Engineering janus interfaces of ceramic electrolyte *via* distinct functional polymers for stable high-voltage Li-metal batteries. J Am Chem Soc, 2019, 141: 9165–9169
38 Luo W, Gong Y, Zhu Y, *et al.* Reducing interfacial resistance between garnet-structured solid-state electrolyte and Li-metal anode by a germanium layer. Adv Mater, 2017, 29: 1606042
39 Wu B, Wang S, Lochala J, *et al.* The role of the solid electrolyte interphase layer in preventing Li dendrite growth in solid-state batteries. Energy Environ Sci, 2018, 11: 1803–1810
40 Zhou W, Wang S, Li Y, *et al.* Plating a dendrite-free lithium anode with a polymer/ceramic/polymer sandwich electrolyte. J Am Chem Soc, 2016, 138: 9385–9388
41 He M, Cui Z, Chen C, *et al.* Formation of self-limited, stable and conductive interfaces between garnet electrolytes and lithium anodes for reversible lithium cycling in solid-state batteries. J Mater Chem A, 2018, 6: 11463–11470
42 Li Y, Xu B, Xu H, *et al.* Hybrid polymer/garnet electrolyte with a small interfacial resistance for lithium-ion batteries. Angew Chem Int Ed, 2017, 56: 753–756
43 Fu J, Yu P, Zhang N, *et al. In situ* formation of a bifunctional interlayer enabled by a conversion reaction to initiatively prevent lithium dendrites in a garnet solid electrolyte. Energy Environ Sci, 2019, 12: 1404–1412
44 Han X, Gong Y, Fu KK, *et al.* Negating interfacial impedance in garnet-based solid-state Li metal batteries. Nat Mater, 2017, 16: 572–579
45 Shao Y, Wang H, Gong Z, *et al.* Drawing a soft interface: An effective interfacial modification strategy for garnet-type solid-state Li batteries. ACS Energy Lett, 2018, 3: 1212–1218
46 Parejiya A, Amin R, Essehli R, *et al.* Electrochemical healing of dendrites in garnet-based solid electrolytes. ACS Energy Lett, 2020, 5: 3368–3373
47 Qin Z, Xie Y, Meng X, *et al.* Recycling garnet-type electrolyte toward superior cycling performance for solid-state lithium batteries. Energy Storage Mater, 2022, 49: 360–369
48 Nowroozi MA, Waidha AI, Jacob M, *et al.* Towards recycling of LLZO solid electrolyte exemplarily performed on LFP/LLZO/LTO cells. ChemistryOpen, 2022, 11: e202100274
49 Wang T, Song Z, Zhang Y, *et al.* Direct recycling of shorted solid-state electrolytes enabled by targeted recovery. Energy Storage Mater, 2022, 52: 365–370
50 Li Y, Cao Y, Guo X. Influence of lithium oxide additives on densification and ionic conductivity of garnet-type $Li_{6.75}La_3Zr_{1.75}Ta_{0.25}O_{12}$ solid electrolytes. Solid State Ion, 2013, 253: 76–80

Acknowledgements This work was partially supported by Shanghai Rising-Star Program (20QA1406600). We also acknowledge the Centre for High-resolution Electron Microscopy (C*h*EM), School of Physical Science and Technology, ShanghaiTech University (EM02161943), Shanghai Science and Technology Plan (21DZ2260400) and Double-Class Initiative Fund of ShanghaiTech University for support.

Author contributions Chen S and Hu X contributed to the experiments and editing; Nie L contributed to the discussion; Yu Y and Liu W were in charge of the scientific research project. All authors contributed to the general discussion.

Conflict of interest The authors declare that they have no conflict of interest.

Supplementary information Supporting data are available in the online version of the paper.

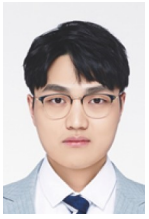

Shaojie Chen received his BS degree in materials science and engineering from Zhejiang Sci-Tech University in 2018. He then joined the School of Physical Science and Technology at ShanghaiTech University under the supervision of Prof. Wei Liu. His research interests focus on solid-state lithium metal batteries and lithium-sulfur batteries.

Xiangchen Hu received his BE degree in materials science and engineering from Shanghaitech University in 2018. He then joined the School of Physical Science and Technology at Shanghaitech University under the supervision of Prof. Yi Yu. His research focuses on the aberration-corrected TEM characterization on beam-sensitive materials (halide perovskite and lithium batteries).

Wei Liu received her BS degree in materials physics from Beijing Normal University in 2008 and her PhD degree in materials science and engineering from Tsinghua University in 2013. She visited the University of Tokyo during 2010–2011. From 2013 to 2017, she was a postdoctoral scholar at Stanford University. She joined ShanghaiTech University as an assistant professor in 2017. Her research interests cover the area of solid-state ionics and nanotechnology, with a focus on the studies of lithium batteries.

通过热愈合方法回收被锂枝晶刺穿的石榴石型固态电解质

陈邵杰[1†], 胡祥辰[1†], 聂璐[1], 于奕[1,3], 刘巍[1,2,3*]

摘要 固态锂金属电池(SSLMBs)因其高安全性和潜在的高能量密度引起了广泛的兴趣. 然而, 锂枝晶在固态电解质中的生长严重阻碍了SSLMBs的实际应用. 在本文中, 我们开发了一种简单的方法, 通过热处理修复和回收被锂枝晶刺穿的石榴石氧化物电解质. 与初始对照样相比, 回收后的石榴石电解质表现出更高的相对密度、离子电导率和临界电流密度. 热愈合是基于树突状锂枝晶和空气间的反应产物, 其有助于在热处理过程中石榴石电解质的进一步致密化. 这项工作为石榴石型固态电解质的回收利用开辟了一条新的途径.

